Materials Science and Engineering A 530 (2011) 548–558

Contents lists available at SciVerse ScienceDirect

Materials Science and Engineering A

journal homepage: www.elsevier.com/locate/msea

Superplasticity governed by effective grain size and its distribution in fine-grained aluminum alloys

F.C. Liu, Z.Y. Ma*

Shenyang National Laboratory for Materials Science, Institute of Metal Research, Chinese Academy of Sciences, 72 Wenhua Road, Shenyang 110016, China

ARTICLE INFO

Article history:
Received 17 March 2011
Received in revised form 19 July 2011
Accepted 11 October 2011
Available online 17 October 2011

Keywords:
Aluminum alloys
Superplasticity
Grain growth
Friction stir processing

ABSTRACT

Although many efforts have been made to improve superplasticity in aluminum alloys by reducing grain size, the present study indicated that just reducing grain size was not sufficient. Three different grain-sized Al–Mg–Sc alloys with a similar misorientation distribution were fabricated by friction stir processing (FSP) and subjected to superplastic investigation. It was revealed that the medium-grained sample exhibited the largest elongation at the highest strain rate due to the optimum combination of proper fine grain and thermal stability. In-depth analyses showed that superplasticity was governed by the effective grain size (d^{eff}) and its distribution just before tension rather than the initial grain size (d^{ini}). The analyses on the superplastic data indicated that the large variation range in the dimensionless constant for superplastic deformation of FSP aluminum alloys was associated with the use of d^{ini} rather than d^{eff}. A modified constitutive equation was developed to elucidate the d^{eff} dependencies of superplastic flow stress which contributed to obtaining the true dimensionless constant and supporting the suggestion that the enhanced kinetics of grain boundary sliding was associated with high fraction of high-angle grain boundaries.

1. Introduction

Superplasticity refers to the ability of a crystalline material to exhibit very high tensile elongations prior to failure. This phenomenon has considerable industrial potential to manufacture complex sheet structures [1]. For most conventional superplastic metals, superplasticity usually occurs in the low strain rate ranging from 10^{-5} to $10^{-3}\,s^{-1}$, and industrial superplastic forming operations are therefore relatively slow with a typical component forming times of ≥30 min. Such a long forming time necessarily precludes the use of superplastic forming in the fabrication of low-cost high volume components for a wide range of industrial applications. Therefore, high strain rate superplasticity (HSRS), at or above $10^{-2}\,s^{-1}$, is desired to increase the utilization of superplastic forming.

The constitutive relationship for superplasticity in fine-grained aluminum alloys can be expressed as [2]

$$\dot{\varepsilon} = A\frac{D_o Eb}{kT}\exp\left(-\frac{84,000}{RT}\right)\left(\frac{b}{d}\right)^2\left(\frac{\sigma-\sigma_o}{E}\right)^2, \quad (1)$$

where $\dot{\varepsilon}$ is the strain rate, A is a constant, D_o is the pre-exponential constant for diffusivity, E is Young's modulus, b is Burger's vector, k is Boltzmann's constant, T is the absolute temperature, R is the gas constant, d is the grain size, σ is the applied stress, and σ_o is the threshold stress. The dimensionless constant A for superplastic deformation of fine grained aluminum alloys is usually in the range of 25–50 [2,3]. Eq. (1) shows that a reduction in the grain size by one order of magnitude will lead to an increase in the strain rate by two orders of magnitude associated with optimum superplastic flow at a constant temperature. Therefore, decreasing the grain size in the structure has become the main idea for searching for structural conditions for HSRS.

Some processes, such as equal-channel-angular pressing (ECAP) [4–6], high pressure torsion [7], cold rolling [8,9], and thermo-mechanical treatment [10] have been used to reduce the grain size to submicrometer range through the imposition of severe plastic deformation. These ultrafine-grained (UFG) aluminum alloys exhibited a good thermal stability and HSRS at high temperatures. However, the optimum strain rates of the UFG aluminum alloys lie in the vicinity of $10^{-2}\,s^{-1}$ and differ insignificantly from those for some fine-grained materials [11]. Many experiments have revealed that the best characteristics of the superplasticity are not observed in the most finely grained materials but in materials with a moderate grain size [12]. It seems that this phenomenon disobeys explanation in the framework of the traditional description of the superplasticity.

Recently, Chuvil'deev et al. [12] developed a model which made it possible to calculate the optimum grain size for a maximum superplasticity. In their approach, the grain boundary sliding (GBS) requires the simultaneous occurrence of "shears" along grain

* Corresponding author. Tel.: +86 24 83978908; fax: +86 24 83978908.
E-mail address: zyma@imr.ac.cn (Z.Y. Ma).

0921-5093/$ – see front matter © 2011 Elsevier B.V. All rights reserved.
doi:10.1016/j.msea.2011.10.018

boundaries and an accommodation of these "shears" at triple junctions. It is needed to maintain a nonequilibrium state of grain boundaries for the development of the intrinsic GBS under deformation. A decrease in the grain size favors the process of the accommodation of GBS, but hinders the maintenance of the nonequilibrium state of grain boundaries. The competition of these processes is responsible for the effect of the optimum grain size on the superplastic deformation.

Friction stir processing (FSP) is an effective technique for producing superplastic aluminum alloys with equiaxed fine-grained structure and predominant high-angle grain boundaries (HAGBs) [13]. The fine-grained FSP aluminum alloys [11,13,14] exhibited HSRS with elongation higher than 1000%. The UFG FSP aluminum alloys produced using special tools or with rapid cooling exhibited low-temperature superplasticity (LTSP) [15–19]. The optimum strain rate for superplasticity as well as the maximum elongation increased with the increasing of temperature. The ductility fell off sharply with an associated rising in flow stress due to abnormal grain growth (AGG) at critical temperatures in some UFG alloys. As a result, the increase of the optimum strain rate and the maximum elongation was limited. By comparison, some UFG FSP aluminum alloys with excellent thermal stability showed elongation higher than 1000% at an exceptional high strain rate of $1\,s^{-1}$ [20].

The above superplastic investigations demonstrated that the effect of the grain size on superplasticity is complex. Furthermore, the initial grain size is generally used in describing the superplastic behavior of the fine-grained aluminum alloys. However, due to the grain growth on heating to superplastic temperature, it is not proper to use the initial grain size. Therefore, the existing theories often cannot account for the relationship between grain size and superplasticity.

Besides the grain size, the grain size distribution is also a key parameter which significantly influences the superplasticity [21–23]. If the grain size distribution is wide, the large grains may deform mainly by dislocation creep during superplastic deformation which is expected to decrease the plastic stability of the alloy. However, in most previous studies, the microstructure was generally reduced to a mean grain size. In consequence, such a treatment cannot predict the effect of microstructural heterogeneities on the superplastic behavior.

In this study, three different grain-sized Al–Mg–Sc samples produced by changing FSP parameters were subjected to superplastic investigation. The aim is to (a) examine the grain structure and grain boundary characters of the samples produced at different FSP parameters, and (b) compare the superplastic behaviors of the fine, medium and coarse grain-sized aluminum alloys, and (c) elucidate the essential factors which govern superplasticity.

2. Experimental

Extruded Al–5.33Mg–0.23Sc–0.49Mn–0.14Fe–0.06Zr (in wt.%) plates were used in this study. FSP was carried out on the extruded plates using a steel tool with a concave shoulder 14 mm in diameter and a threaded conical pin 5 mm in root diameter and 4.5 mm in length. Three different rotation rate–travel speed combinations, i.e. 400 rpm–100 mm/min, 600 rpm–25 mm/min and 800 rpm–25 mm/min were used to generate the microstructures with different grain sizes. Microstructural characterization was performed on the cross-section of the stir zone (SZ) transverse to the FSP direction by scanning electron microscopy (SEM). The samples for SEM were lightly electropolished to produce a strain-free surface. Electron backscatter diffraction (EBSD) orientation maps were obtained using a ZEISS SUPRA 35, operated at 20 kV, and interfaced to an HKL Channel EBSD system.

Dog-bone shaped superplastic tensile specimens (2.5 mm gage length, 1.4 mm gage width and 1.0 mm gage thickness) were electro-discharge machined from the SZ of the FSP samples transverse to the FSP direction. These specimens were subsequently ground and polished to a final thickness of ~0.8 mm. Constant crosshead speed tensile tests were conducted using INSTRON 5848 micro-tester. Each specimen was held at the testing temperature for about 15 min in order to reach thermal equilibrium.

To check on the thermal stability of the fine-grained microstructure introduced by FSP, small specimens with dimensions of 8 mm × 8 mm × 10 mm cutting from the SZs were statically annealed for 15 min at temperatures from 400 to 550 °C, respectively, and then cooled rapidly in water to provide the microstructure information of the FSP samples just before tensile test at various temperatures. The samples were polished with colloidal silica, and then etched in 10% phosphoric acid at 50 °C. For each annealed sample, Sisc IAS metallography analysis software was used to determine the grain size distribution. Over 3000 grains per sample were measured to obtain accurate statistics. Eqs. (2) and (3) were used to compute the mean grain size ($\bar{d}$) and standard deviation (P).

$$\bar{d} = \frac{\sum n_i d_i}{\sum n_i}, \tag{2}$$

$$P = \left[\frac{\sum n_i (d_i - \bar{d})^2}{\sum n_i} \right]^{1/2}. \tag{3}$$

3. Results

3.1. Microstructural characteristics

Fig. 1 shows the microstructure of the FSP Al–Mg–Sc samples obtained by EBSD maps. These maps show similar homogeneous microstructures consisting of fine equiaxed grains that differ mainly in the size of the grains. The average grain size was determined to be 1.6, 2.6 and 2.9 μm for processing parameters of 400 rpm–100 mm/min, 600 rpm–25 mm/min and 800 rpm–25 mm/min, respectively (hereafter referred to as 1.6, 2.6 and 2.9 μm Al–Mg–Sc). The misorientation angle histograms of the FSP Al–Mg–Sc samples are shown in Fig. 2. The three samples exhibited a similar misorientation distribution which is very close to the theoretical distribution for a random polycrystal of cubic structure predicted by Mackenzie [24]. The fraction of HAGBs was in the range of 95–98% and very close to the random grain assembly (97%). The average misorientation angle was determined to be 39.1–41.3° and very close to 40.7° for the random distribution. Furthermore, it was revealed that a random texture characterized these three FSP Al–Mg–Sc samples and no significant differences could be observed among them (Fig. 3). The textures of the three samples were quite weak with a maximum density of 2.40.

3.2. Stability of the grains in static annealing

The results from the annealing experiments are shown in Fig. 4. It is apparent from this plot that the rapid grain growth occurred at temperatures above ~475 °C for the 1.6 μm Al–Mg–Sc, ~500 °C for the 2.6 μm Al–Mg–Sc and ~525 °C for the 2.9 μm Al–Mg–Sc. The 1.6 μm Al–Mg–Sc exhibited a higher grain growth rate than the 2.6 and 2.9 μm Al–Mg–Sc at the temperature range of 400–525 °C. Above 500 °C, the 1.6 μm Al–Mg–Sc showed a larger average grain size than the 2.6 and 2.9 μm Al–Mg–Sc.

Typical optical micrographs of the 1.6 μm Al–Mg–Sc at 475 °C and 500 °C, the 2.6 μm Al–Mg–Sc at 475 °C and the 2.9 μm Al–Mg–Sc at 500 °C are shown in Fig. 5. The 2.6 μm Al–Mg–Sc

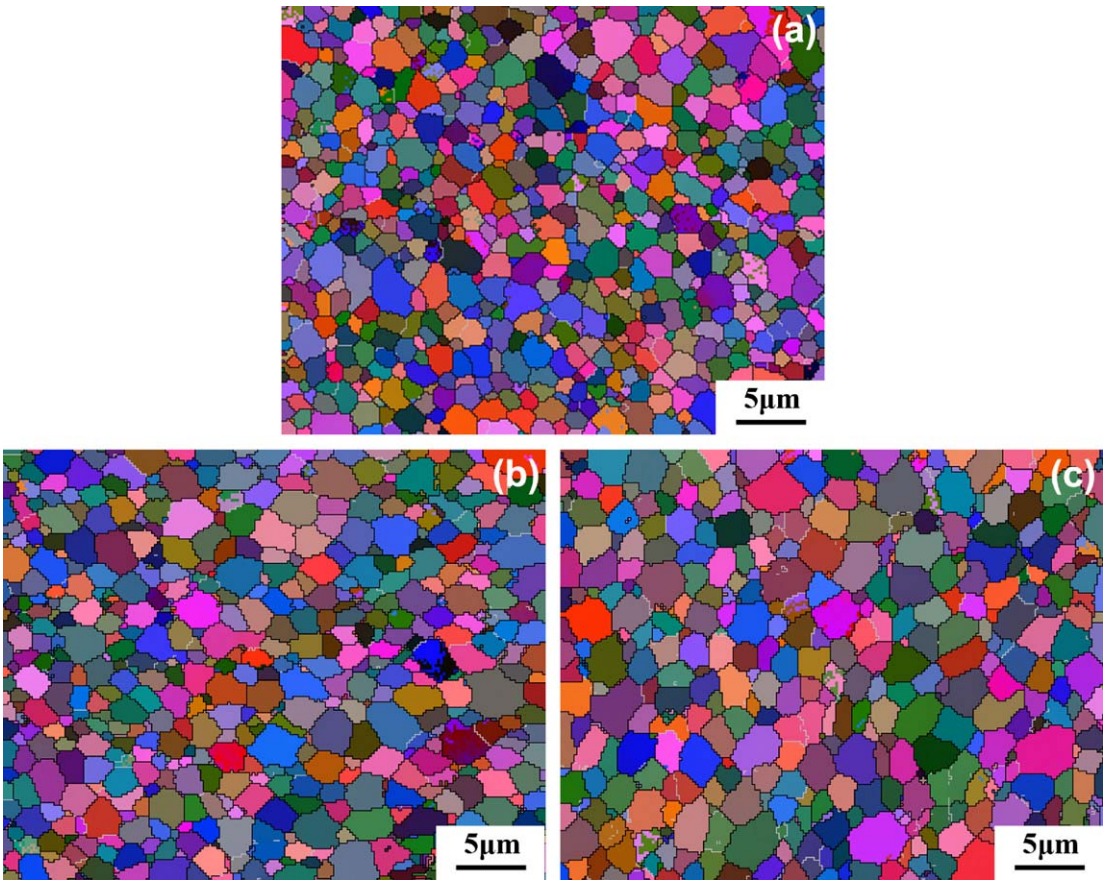

Fig. 1. EBSD maps showing grain structure of FSP Al–Mg–Sc: (a) 1.6 μm, (b) 2.6 μm and (c) 2.9 μm.

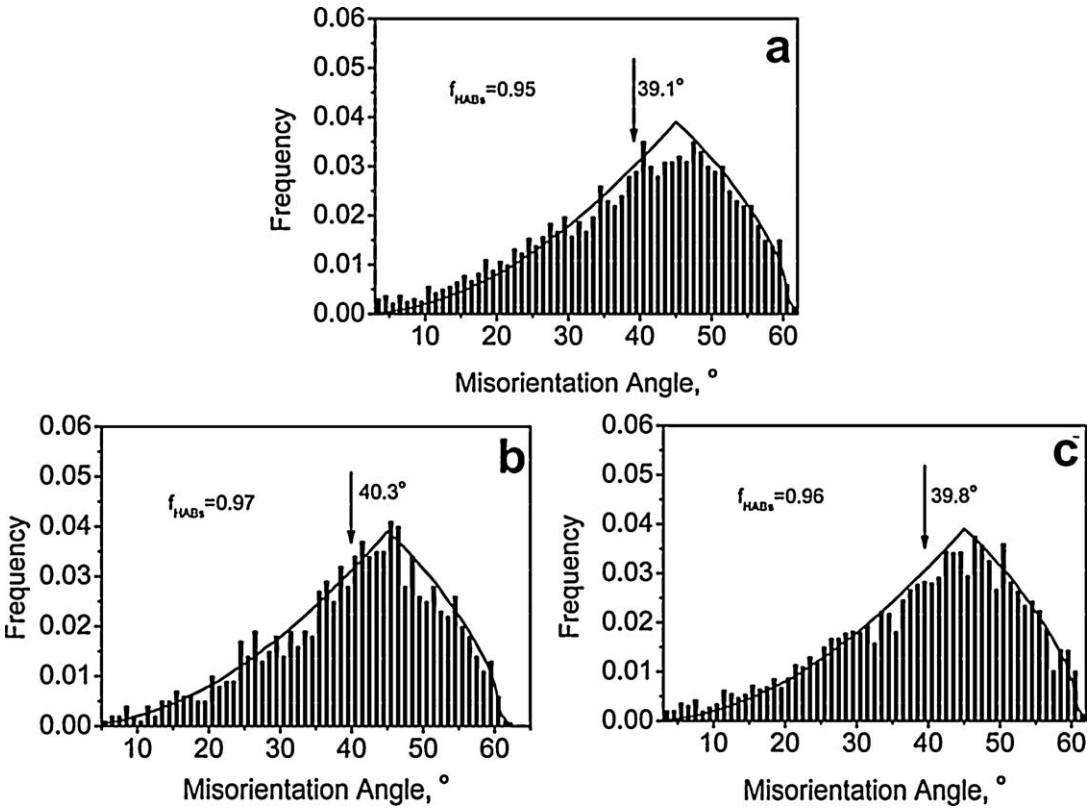

Fig. 2. Boundary misorientation angle distribution of (a) 1.6 μm Al–Mg–Sc, (b) 2.6 μm Al–Mg–Sc and (c) 2.9 μm Al–Mg–Sc.

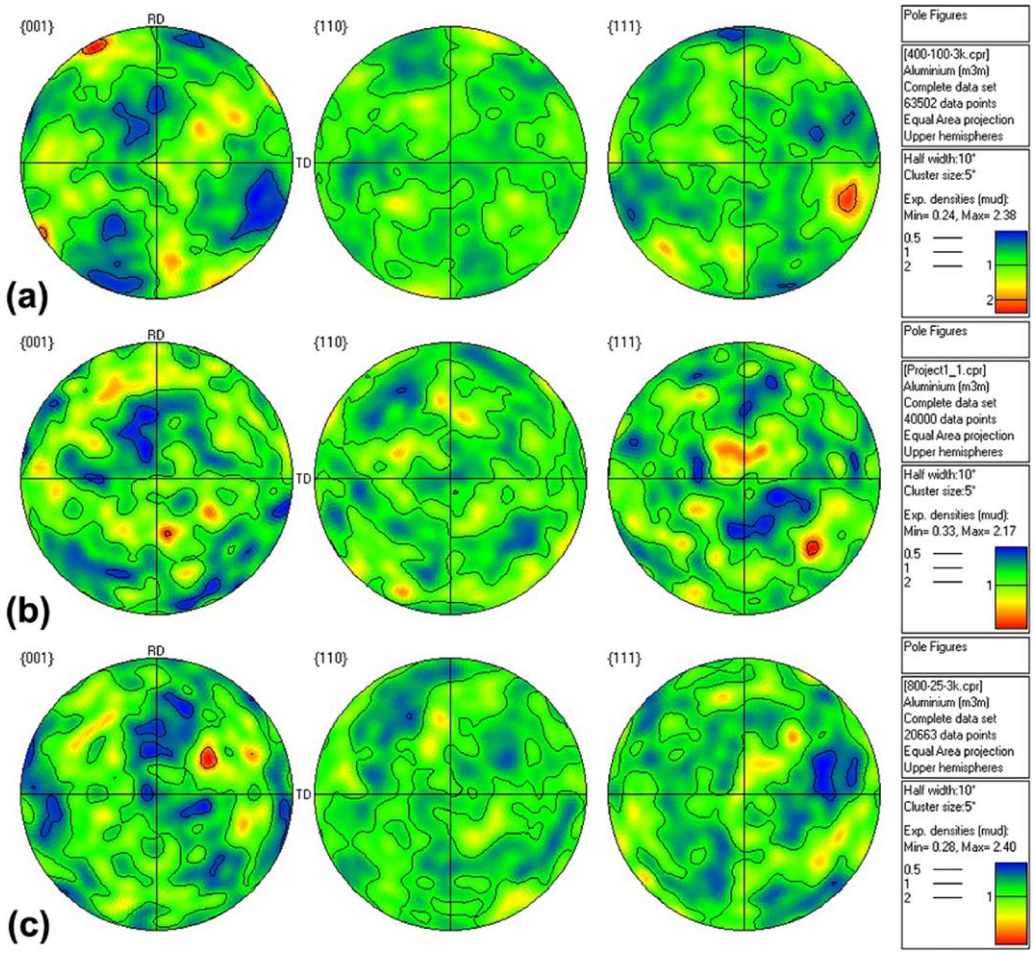

Fig. 3. Pole figures of (a) 1.6 μm Al–Mg–Sc, (b) 2.6 μm Al–Mg–Sc and (c) 2.9 μm Al–Mg–Sc (sample surface was perpendicular to the FSP direction).

showed a more homogeneous microstructure than the 1.6 μm Al–Mg–Sc at 475 °C. Similarly, the 2.9 μm Al–Mg–Sc also showed a more homogeneous microstructure than the 1.6 μm Al–Mg–Sc at 500 °C.

3.3. Superplasticity at elevated temperatures

Fig. 6a shows the variation of superplastic elongation with the strain rate in the 1.6 μm Al–Mg–Sc at different temperatures. An optimum strain rate of $3 \times 10^{-2}\ s^{-1}$ for maximum elongation was observed in the temperature range from 400 to 475 °C. With increasing temperature from 400 to 450 °C, the maximum elongation increased from 930 to 1480%. However, further increasing the temperature from 450 to 525 °C resulted in a monotonic decrease in the maximum elongation. The largest elongation of 1480% was achieved at 450 °C and $3 \times 10^{-2}\ s^{-1}$. Fig. 6b shows the variation of superplastic elongation with the strain rate at different temperatures for the 2.6 μm Al–Mg–Sc. A temperature increase from 425 to 450 °C resulted in an increase in the optimum strain rate for superplasticity as well as the maximum elongation. The largest elongation of 2150% was achieved at 450 °C and $1 \times 10^{-1}\ s^{-1}$. However, with increasing the temperature from 450 to 525 °C, the maximum elongation decreased from 2150% to 1280%. Fig. 6c shows the variation of superplastic elongation with the strain rate at different temperatures for the 2.9 μm Al–Mg–Sc. At 450 °C, the FSP Al–Mg–Sc exhibited a maximum superplasticity of 1250% at an initial strain rate of $3 \times 10^{-2}\ s^{-1}$. With increasing the temperature to 475 °C, the largest ductility and optimum strain rate increased to 1300% and $1 \times 10^{-1}\ s^{-1}$, respectively. However, further increasing the temperature to 500 °C increased the largest ductility to 1550% but decreased the optimum strain rate to $3 \times 10^{-2}\ s^{-1}$. At 525 °C, a maximum elongation of 1850% was observed at a further reduced strain rate of $1 \times 10^{-2}\ s^{-1}$.

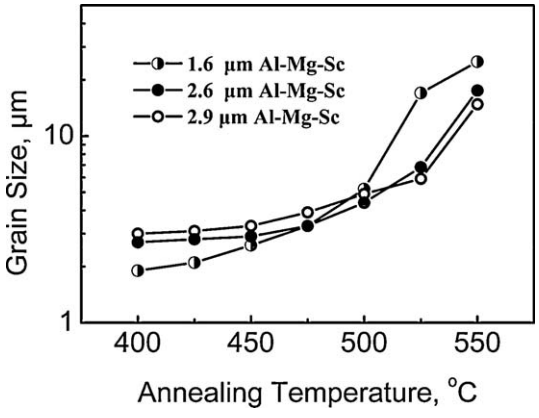

Fig. 4. Grain size as a function of annealing temperature for three FSP samples.

Fig. 7 shows the effect of temperature on the superplastic ductility of the FSP Al–Mg–Sc at an initial strain rate of $1 \times 10^{-1}\ s^{-1}$. The 1.6 μm Al–Mg–Sc exhibited superplastic ductility over a wide temperature range of 325–550 °C. The maximum ductility of 1350% appeared at 450 °C. The 2.6 μm Al–Mg–Sc exhibited enhanced ductility of >1500% at the temperature range of 450–500 °C, and a maximum ductility of 2150% was obtained at 450 °C. Increasing the

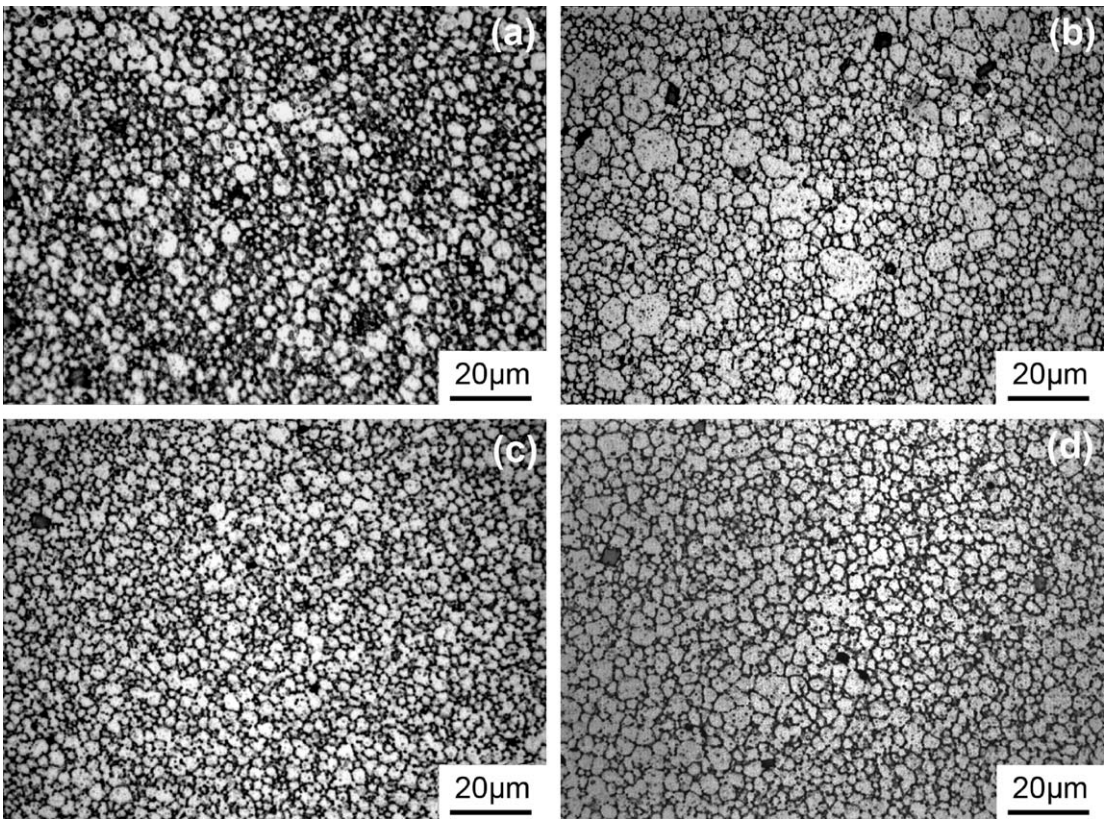

Fig. 5. Typical optical micrographs showing grain structure: (a) 1.6 μm Al–Mg–Sc annealed at 475 °C, (b) 1.6 μm Al–Mg–Sc annealed at 500 °C, (c) 2.6 μm Al–Mg–Sc annealed at 475 °C and (d) 2.9 μm Al–Mg–Sc annealed at 500 °C.

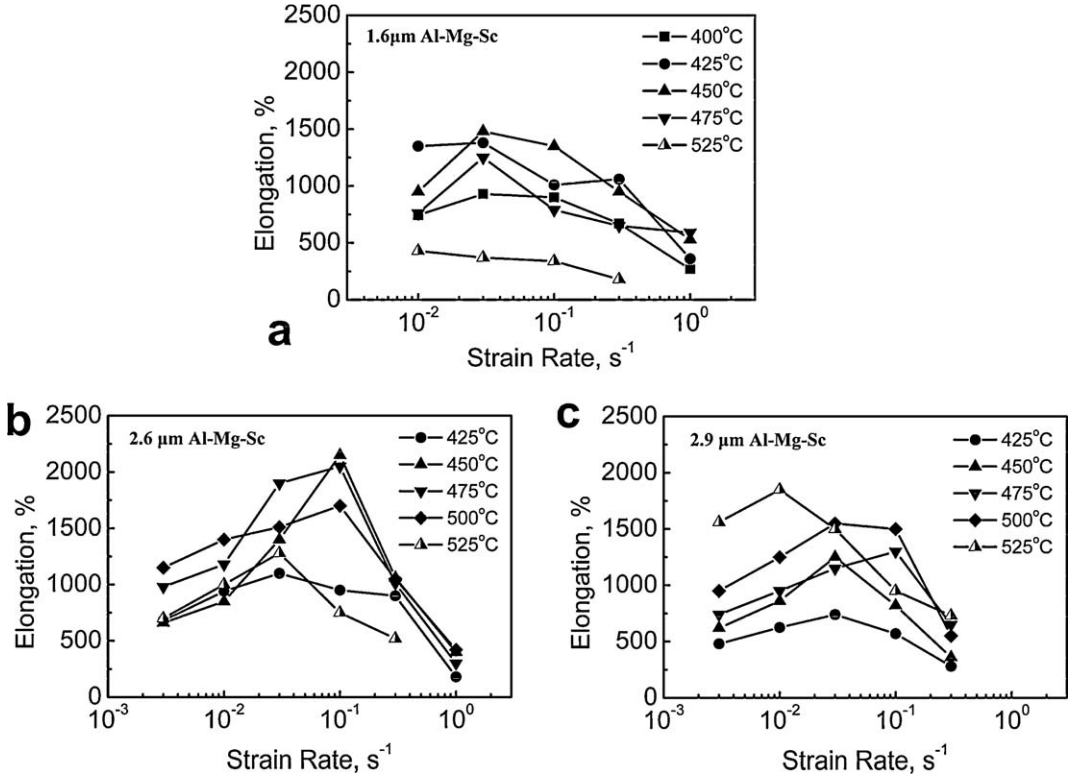

Fig. 6. Variation of elongation with initial strain rate at various test temperatures for (a) 1.6 μm Al–Mg–Sc, (b) 2.6 μm Al–Mg–Sc and (c) 2.9 μm Al–Mg–Sc.

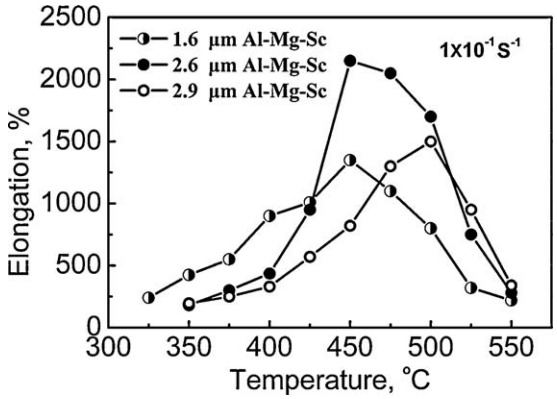

Fig. 7. Variation in elongation with test temperature at initial strain rate of 1×10^{-1} s^{-1} for three FSP samples.

grain size to 2.9 μm resulted in a maximum ductility of 1500% at a high temperature of 500 °C.

Fig. 8 shows the variation of flow stress (at true strain of 0.1) with the initial strain rate for the FSP Al–Mg–Sc samples. Strain rate sensitivity (m) of ~0.5 was observed in the optimum strain rate range for the three FSP Al–Mg–Sc samples. It is interesting to note that the flow stress decreased with increasing temperature for the 2.9 μm Al–Mg–Sc, but exhibited an inverse trend at 525 °C for the 1.6 and 2.6 μm Al–Mg–Sc.

4. Discussion

4.1. Microstructural characteristics

The three FSP Al–Mg–Sc samples exhibited a similar grain boundary misorientation distribution, i.e. a close match with the theoretical distribution of grain boundary misorientation angles for a random polycrystal of cubic structure predicted by Mackenzie [24]. Similar boundary misorientation distribution was also observed in UFG FSP Al–Mg–Sc alloys with 95% of HAGBs [17,19] and FSW 7071Al with 80–90% of HAGBs [25]. Recently, Gerlich et al. [26] reported that the fraction of HAGBs in a friction stir spot welded 2024Al varied from 67.5 to 95.9% when the tool rotation rate decreased from 1125 to 750 rpm. All these results suggest that FSP aluminum alloys contained a high fraction of HAGBs. It should be noted that the FSP Al–Mg–Sc samples in this study exhibited similar grain shape, boundary misorientation distribution and texture, indicating that the initial microstructures for superplastic investigation in these FSP samples differ only in the grain size. Such sort of microstructures have been rarely reported in previous literatures because the variation in the grain size usually results in a change in the grain shape, misorientation distribution and texture to a certain extent.

4.2. Conception of effective grain size

The variations of elongation with the strain rate for different grain-sized samples at 425, 475 and 525 °C are shown in Fig. 9. At 425 °C, the elongation increased with decreasing the initial grain size at investigated strain rates. This phenomenon is in good agreement with the traditional description of the superplasticity. At 475 °C, compared with the 1.6 and 2.9 μm Al–Mg–Sc, the 2.6 μm Al–Mg–Sc exhibited the largest elongation at the strain rates from 3×10^{-3} to 3×10^{-1} s^{-1}. It seems that this phenomenon is consistent with the occurrence of the optimum grain size for the superplasticity [12]. However, at 525 °C, the 2.9 μm Al–Mg–Sc exhibited the largest elongation at the strain rates from 3×10^{-3} to 3×10^{-1} s^{-1} which defied the explanations in the previous works.

In order to uncover the essential factors that govern superplastic deformation, a new conception of "effective grain size" is proposed in this study. When annealed at temperatures <425 °C, the grain size of the 1.6 μm Al–Mg–Sc was smaller than that of other samples (Fig. 4). Therefore, the 1.6 μm Al–Mg–Sc exhibited a higher elongation at temperatures <425 °C. When annealed at 475 °C, the 2.6 μm Al–Mg–Sc showed a finer grain size than the 2.9 μm Al–Mg–Sc, hence exhibiting a higher elongation than the 2.9 μm Al–Mg–Sc. It is noted that the average grain size of the 1.6 μm Al–Mg–Sc was the same as that of the 2.6 μm Al–Mg–Sc at 475 °C (Fig. 4), but the 2.6 μm Al–Mg–Sc exhibited a higher elongation than the 1.6 μm Al–Mg–Sc. A reasonable explanation will be detailedly discussed in Section 4.4. At 525 °C, the 2.9 μm Al–Mg–Sc which has the largest initial grain size exhibited the largest elongation because of its finest grain size just before deformation. These demonstrate that the superplastic elongation is controlled by the grain size just before deformation rather than the initial one. Therefore, the grain size just before deformation can be called as effective grain size d^{eff}.

4.3. d^{eff} governing superplasticity in different initial grain-sized samples

Though Section 4.2 has indicated that a smaller d^{eff} not an initial grain size (d^{ini}) resulted in a higher superplasticity at a given temperature, it is not so convenient to determine the d^{eff} as the d^{ini}. Clarifying the relationship among the d^{ini}, d^{eff} and superplasticity will help to understand the effect of the d^{eff} on superplasticity for different grain-sized samples. To facilitate the discussion, the d^{ini} is classified into three groups, i.e. fine (1.6 μm), medium (2.6 μm) and coarse (2.9 μm) depending on their superplastic behavior.

The aluminum alloys with a fine d^{ini} usually exhibited a smaller d^{eff} at lower temperatures. Therefore, the fine-grained structure is beneficial to obtaining excellent superplasticity at lower temperatures. For example, the UFG 7075Al, Al–Mg–Sc, and Al–Cu–Zr exhibited LTSP at 200 °C (or thereabouts) [17,18,27]. However, the low deformation temperature reduced the optimum strain rate of the UFG materials because superplasticity is usually rate controlled by either diffusion or dislocation motion [28]. Additionally, the threshold stress values usually increased with decreasing the deformation temperature, resulting in relatively low strain rate sensitivities at lower temperatures [17–19]. Thus, the superplasticity of the aluminum alloys at lower temperatures is lower than that at higher temperatures because of its low resistance to the development of the necking.

The high temperature superplasticity of aluminum alloys with a fine d^{ini} tends to fall into two groups. For the aluminum alloys with an excellent thermal stability, HSRS with a high elongation can be achieved at higher temperatures due to its small d^{eff}. One example is that the UFG FSP Al–4Mg–1Zr exhibited a maximum ductility of 1404% at high strain rate of 1 s^{-1} even at 425 °C because the d^{eff} was smaller than 1 μm [20]. For most of aluminum alloys with fine d^{ini}, the d^{eff} usually increased remarkably with increasing temperature. Inhomogeneous grain growth (IGG) even occurred in these materials at higher temperatures. As a result, it is hard to obtain a high superplastic elongation at higher temperatures and higher strain rates in these alloys.

In the present study, the 1.6 μm Al–Mg–Sc with a fine d^{ini} showed a smaller d^{eff} and higher elongations at temperatures lower than 425 °C compared with the 2.6 and 2.9 μm Al–Mg–Sc (Fig. 4). At temperatures higher than 500 °C, IGG developed in the 1.6 μm Al–Mg–Sc (Fig. 5), which resulted in a larger d^{eff} than that in the 2.6 and 2.9 μm Al–Mg–Sc (Fig. 4). Therefore, the 1.6 μm Al–Mg–Sc exhibited a lower elongation at temperatures higher than 500 °C compared with the other two samples.

The aluminum alloys with a medium d^{ini} could exhibit the largest superplastic elongation and the highest optimum strain

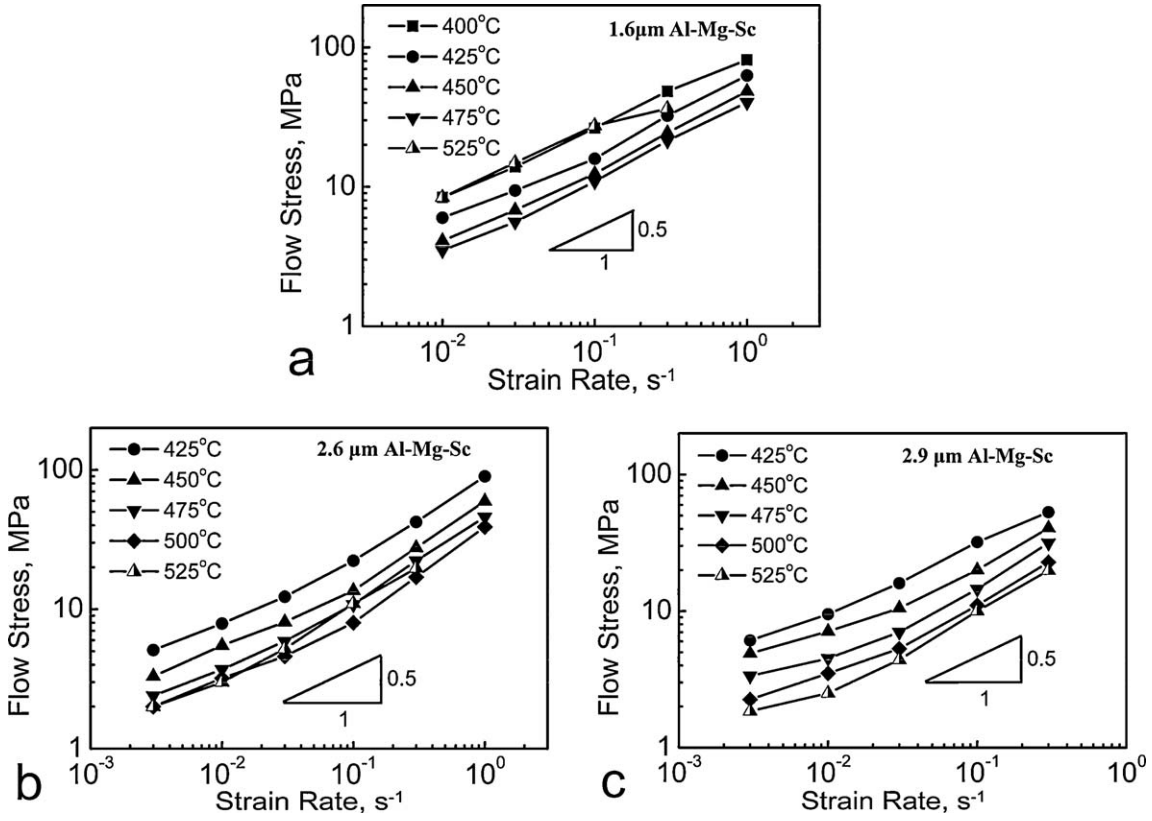

Fig. 8. Variation of flow stress with initial strain rate at various test temperatures for (a) 1.6 μm Al–Mg–Sc, (b) 2.6 μm Al–Mg–Sc, and (c) 2.9 μm Al–Mg–Sc.

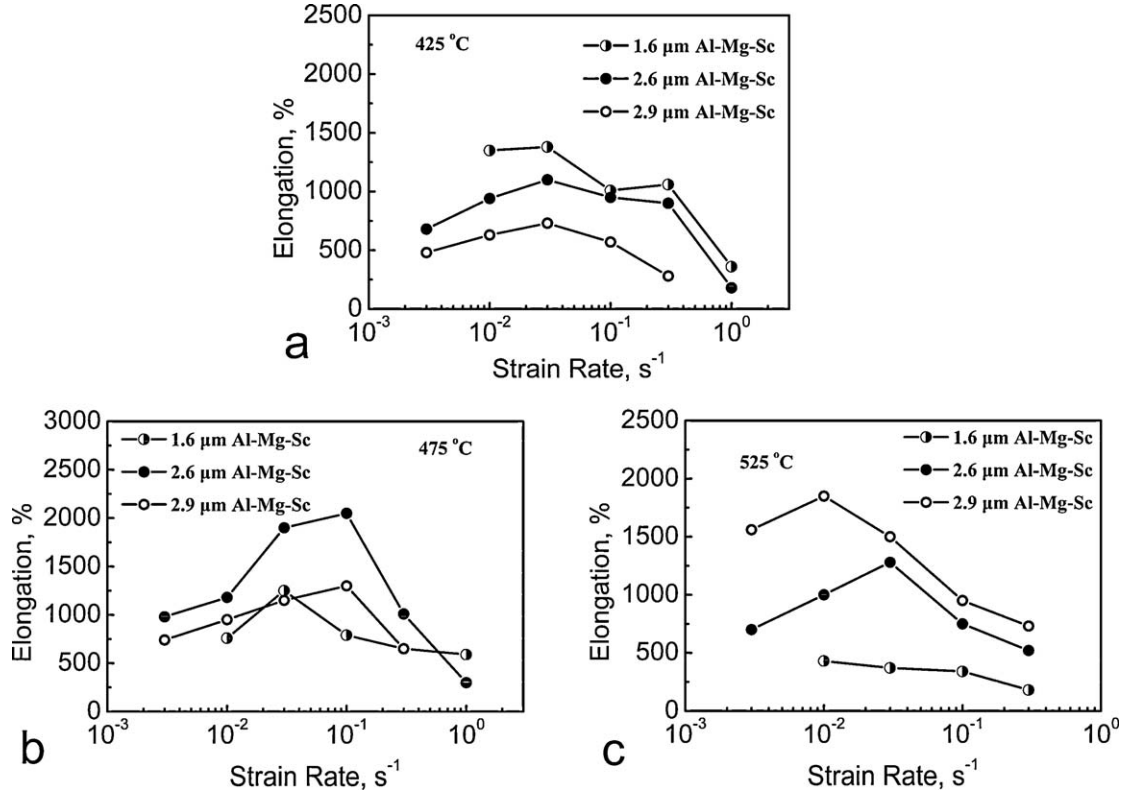

Fig. 9. Variations of elongation with strain rate for different grain-sized alloys at (a) 425 °C, (b) 475 °C, and (c) 525 °C.

Table 1
d^{eff} parameters and statistical data after annealing for 20 min at different temperatures for the three samples.

Sample	Temperature (°C)	Mean d^{eff} (μm)	$d^{eff}_{max}/\overline{d^{eff}}$	Standard deviation, P (μm)	$P/\overline{d^{eff}}$
1.6 μm Al–Mg–Sc	475	3.3	2.7	1.91	0.58
1.6 μm Al–Mg–Sc	500	5.2	2.6	2.89	0.55
2.6 μm Al–Mg–Sc	475	3.3	1.8	1.30	0.39
2.9 μm Al–Mg–Sc	500	4.9	1.8	1.69	0.34

rate at a moderate temperature due to the smallest d^{eff} at this temperature. The 2.6 μm Al–Mg–Sc with a medium-grained structure showed the smallest d^{eff} at 475–500 °C compared with the 1.6 and 2.9 μm Al–Mg–Sc (Fig. 4), and therefore exhibited the largest superplastic elongation and the highest optimum strain rate at 475 °C.

The aluminum alloys with a coarse d^{ini} could show a high superplastic elongation at higher temperatures because the excellent grain stability of these alloys resulted in the smallest d^{eff} at higher temperatures, though it is impossible for these alloys to exhibit superplasticity at lower temperatures. For the 2.9 μm Al–Mg–Sc with a coarse d^{ini}, the d^{eff} was larger than that for the other two samples at temperatures lower than 475 °C. However, at temperatures higher than 525 °C, the d^{eff} was smaller than that for the other two samples because of its slow increase trend. Therefore, the 2.9 μm Al–Mg–Sc exhibited the highest elongation at 525 °C.

4.4. Effect of d^{eff} distribution on superplasticity

Fig. 4 shows that the 1.6 and 2.6 μm Al–Mg–Sc exhibited the same d^{eff} before superplastic deformation at 475 °C. However, the elongation of the 2.6 μm Al–Mg–Sc was twice over the 1.6 μm Al–Mg–Sc at 475 °C and 1×10^{-1} s^{-1} (Fig. 7). Similarly, the 1.6 and 2.9 μm Al–Mg–Sc exhibited similar d^{eff} at 500 °C, but the elongation of the 2.9 μm Al–Mg–Sc was twice over the 1.6 μm Al–Mg–Sc at 500 °C and 1×10^{-1} s^{-1} (Fig. 7). A further understanding of the superplastic difference may be achieved from statistical analyses of the d^{eff} distribution. Fig. 10 shows the d^{eff} distribution of the 1.6 μm Al–Mg–Sc at 475 °C and 500 °C, the 2.6 μm Al–Mg–Sc at 475 °C and the 2.9 μm Al–Mg–Sc at 500 °C. Table 1 summarizes the ratio of the maximum d^{eff} to the mean d^{eff} ($d^{eff}_{max}/\overline{d^{eff}}$) and standard deviation (P).

A comparison of the d^{eff} distribution shows that the 1.6 μm Al–Mg–Sc exhibits a wider d^{eff} distribution, higher $d^{eff}_{max}/\overline{d^{eff}}$ and P values than the 2.6 μm Al–Mg–Sc after annealing at 475 °C. Similarly, the 1.6 μm Al–Mg–Sc also exhibits a wider d^{eff} distribution, higher $d^{eff}_{max}/\overline{d^{eff}}$ and P values than the 2.9 μm Al–Mg–Sc after annealing at 500 °C. This is attributed to the occurrence of IGG in the 1.6 μm Al–Mg–Sc (Fig. 5). These results demonstrate that a concentrative d^{eff} distribution, i.e. smaller $d^{eff}_{max}/\overline{d^{eff}}$ and P values, is beneficial to enhancing superplastic elongation.

Some models have been proposed to predict the effect of microstructural heterogeneities on superplastic deformation [21–23]. Their studies confirmed that different superplastic flows were obtained depending on the grain size distribution, despite the same mean grain size. A microstructure with a broad grain size distribution may result in a significant localization of deformation in the superplastic domain. However, the relationship between microstructural heterogeneities and superplastic elongation was not mentioned in the previous works. The present results confirmed that irrespective of the same mean d^{eff}, a concentrative d^{eff} distribution is beneficial to obtaining high superplastic elongation, which is in good agreement with the previous predictions.

4.5. d^{eff} governing superplastic flow stress

The variations of the flow stress with the strain rate for different grain-sized samples at 425, 475 and 525 °C are shown in Fig. 11. Eq. (1) predicts a linear relationship between the grain size and flow stress at a constant strain rate and temperature. This implies that a decrease in the grain size will result in a concurrent reduction in the flow stress accompanying superplastic deformation. At 425 °C, the flow stress decreased with decreasing the d^{ini} at investigated strain rates, which is in good agreement with the prediction of Eq. (1). However, with increasing the temperature to 475 °C, the 1.6 μm Al–Mg–Sc exhibited the flow stresses similar to those of the 2.6 μm Al–Mg–Sc. At 525 °C, the flow stress decreased with increasing the d^{ini}, which is contrary to the prediction by Eq. (1). This is because that the flow stress was governed by the d^{eff} rather than the d^{ini} at a given temperature. At 525 °C, the d^{eff} of the 1.6 μm Al–Mg–Sc was larger than that of the 2.6 and 2.9 μm Al–Mg–Sc. Therefore, it is not surprising that the flow stress of the 1.6 μm Al–Mg–Sc was larger than that of the 2.6 and 2.9 μm Al–Mg–Sc at 525 °C.

4.6. Effect of d^{ini} and d^{eff} on kinetics of GBS

In analyzing the superplastic data by Eq. (1), usually, the d^{ini} of the superplastic materials is used as the grain size d for convenience. When the deformation temperature is not very high and the materials are thermally stable, the grains usually exhibit limited growth during heating. In this case, the grain size of the superplastic materials before superplastic deformation, i.e. the d^{eff}, is approximately equivalent to the d^{ini}. Therefore, Eq. (1) is able to predict the superplastic flow behaviors by using the d^{ini}. However, the grains of the FSP Al–Mg–Sc have grown significantly before deformation at higher temperatures.

Fig. 12a shows the variation of $\dot{\varepsilon}kTd^2/(G_gEb^3)$ versus σ/E for the 1.6 μm Al–Mg–Sc. The data obtained at temperatures of 400–475 °C fit onto a straight line which can be described by

$$\dot{\varepsilon} = 309\frac{D_oEb}{kT}\exp\left(-\frac{84,000}{RT}\right)\left(\frac{b}{d}\right)^2\left(\frac{\sigma}{E}\right)^2 \quad (4)$$

Clearly, the dimensionless constant in Eq. (4) is much higher than that predicted by Eq. (1). Higher values of the dimensionless constant have been observed in the FSP aluminum alloys [11,29,30]. This enhanced kinetics of GBS for the FSP aluminum alloys was attributed to the high percent of HAGBs produced by FSP [11,13]. However, the superplastic data of the 1.6 μm Al–Mg–Sc obtained at 525 °C fit onto another straight line which can be described by

$$\dot{\varepsilon} = 28\frac{D_oEb}{kT}\exp\left(-\frac{84,000}{RT}\right)\left(\frac{b}{d}\right)^2\left(\frac{\sigma}{E}\right)^2 \quad (5)$$

This lower dimensionless constant of 28 is inconsistent with the enhanced kinetics observed in previous FSP aluminum alloys. Furthermore, the data of the 1.6 μm Al–Mg–Sc cannot fit onto a single straight line, demonstrating that Eq. (1) is unfit to predict its superplastic flow behaviors. The breakdown of the traditional constitutive equation is because that the d^{eff} for GBS is obviously larger than the d^{ini} for the 1.6 μm Al–Mg–Sc.

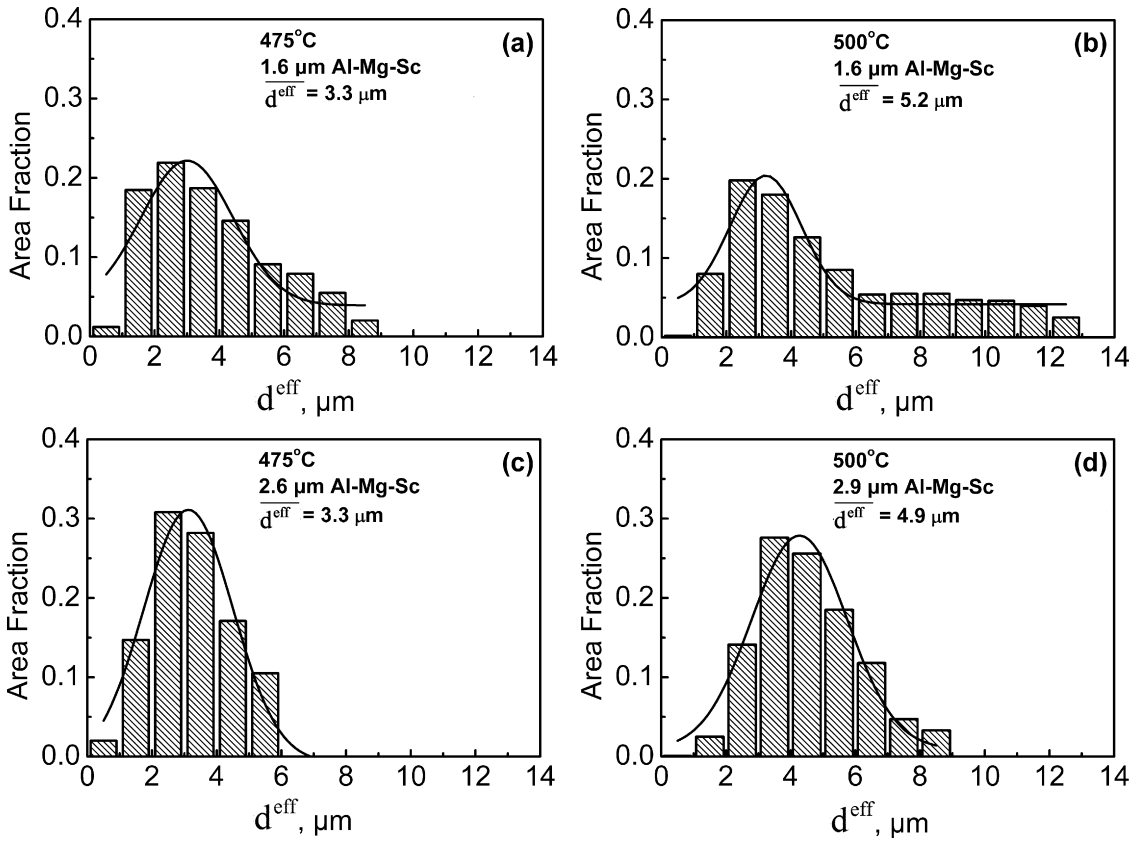

Fig. 10. Grain size distributions for (a) 1.6 μm Al–Mg–Sc annealed at 475 °C, (b) 1.6 μm Al–Mg–Sc annealed at 500 °C, (c) 2.6 μm Al–Mg–Sc annealed at 475 °C and (d) 2.9 μm Al–Mg–Sc annealed at 500 °C.

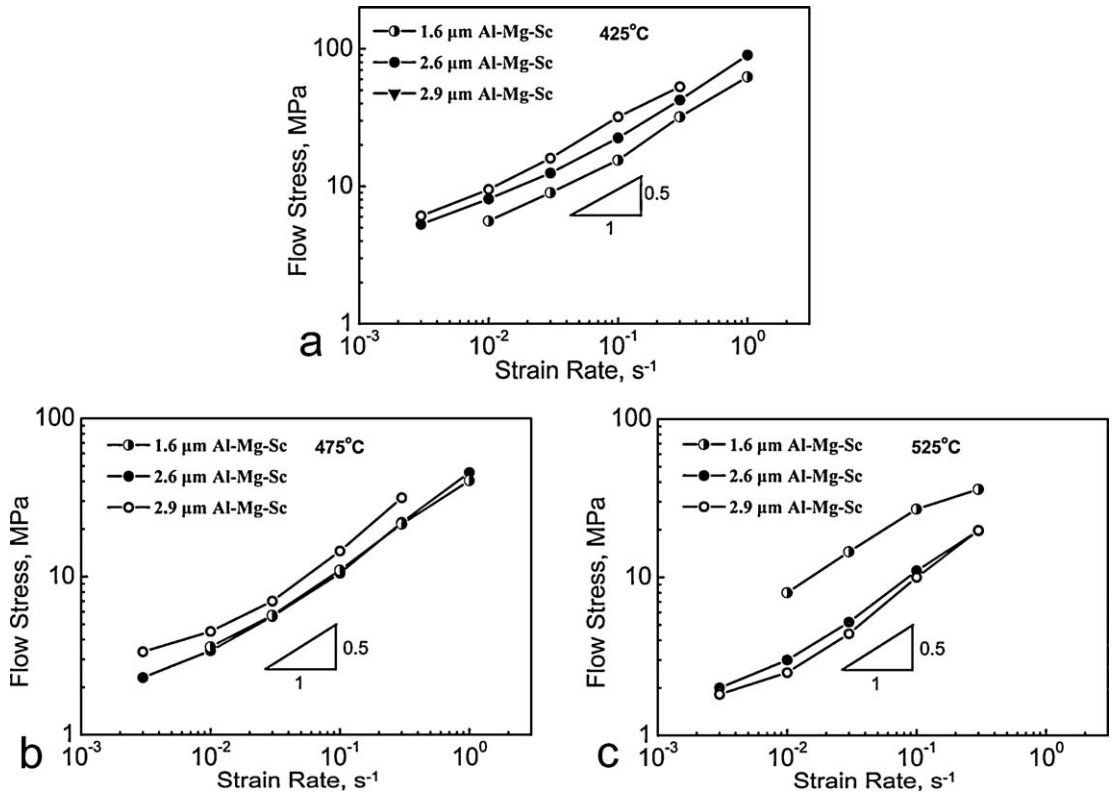

Fig. 11. Variations of flow stress with strain rate for different grain-sized alloys at (a) 425 °C, (b) 475 °C, and (c) 525 °C.

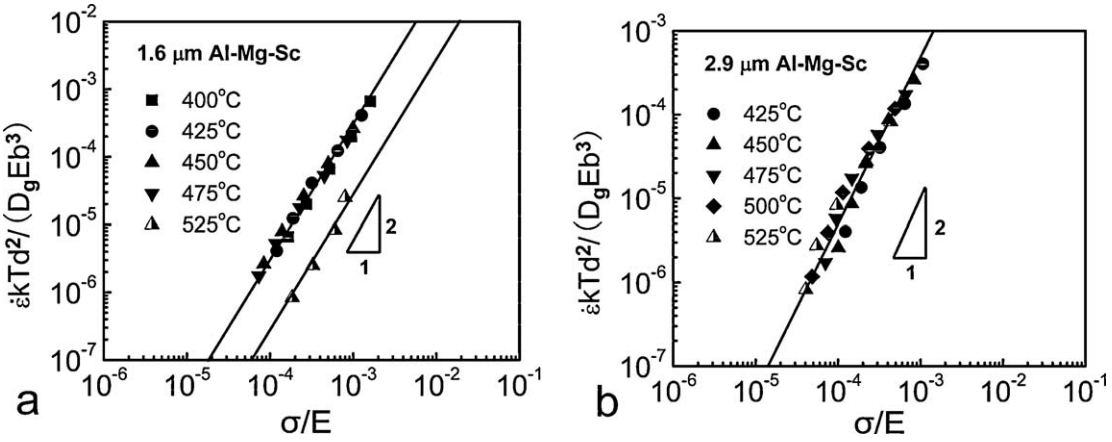

Fig. 12. Variation of $\dot{\varepsilon}kTd^2/(G_gEb^3)$ as a function of σ/E for (a) 1.6 μm Al–Mg–Sc and (b) 2.9 μm Al–Mg–Sc.

Fig. 12b shows the variation of $\dot{\varepsilon}kTd^2/(G_gEb^3)$ versus σ/E for the 2.9 μm Al–Mg–Sc. The superplastic deformation behaviors can be described by

$$\dot{\varepsilon} = 550\frac{D_oEb}{kT}\exp\left(-\frac{84,000}{RT}\right)\left(\frac{b}{d}\right)^2\left(\frac{\sigma}{E}\right)^2 \quad (6)$$

Previous studies showed that the dimensionless constant for superplastic deformation of the FSP aluminum alloys varied in the range of 100–1400 [11,29,30]. However, this large variation in the dimensionless constant has not been well understood. Considering remarkable grain growth in the fine-grained materials at higher temperatures, it is more reasonable to use the d^{eff} instead of the d^{ini} to describe the superplastic behavior of the fine-grained materials.

Fig. 13 shows the variation of $\dot{\varepsilon}kT(d^{\text{eff}})^2/(G_gEb^3)$ versus σ/E. For comparison, the straight line predicted by the traditional constitutive equation for superplasticity in fine-grained aluminum alloys [2] is also included. The data of the three FSP samples fit onto a single straight line which can be described by

$$\dot{\varepsilon} = 1500\frac{D_oEb}{kT}\exp\left(-\frac{84,000}{RT}\right)\left(\frac{b}{d^{\text{eff}}}\right)^2\left(\frac{\sigma}{E}\right)^2 \quad (7)$$

Eq. (7) indicates that GBS is the primary deformation mechanism for the present FSP Al–Mg–Sc. The fitting of all the superplastic data onto a single straight line indicated that the variation of the dimensionless constant in Eqs. (4)–(6) is associated with the use of the d^{ini}. The true dimensionless constant obtained by using the d^{eff} is higher than that by using d^{ini}. The true dimensionless constant

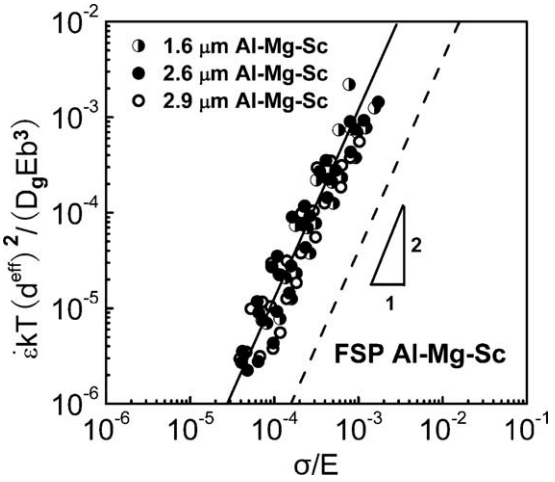

Fig. 13. Variation of $\dot{\varepsilon}kTd^{\text{eff}2}/(G_gEb^3)$ as a function of σ/E for FSP Al–Mg–Sc.

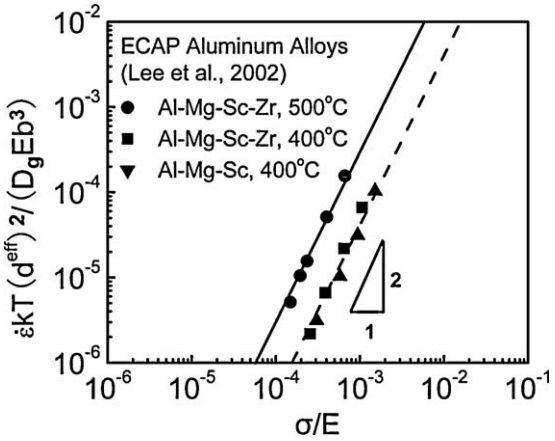

Fig. 14. Variation of $\dot{\varepsilon}kTd^{\text{eff}2}/(G_gEb^3)$ as a function of σ/E for ECAP aluminum alloys.

of 1500 is significantly larger than the prediction (25–50) by Eq. (1), indicating significantly enhanced deformation kinetics in the FSP Al–Mg–Sc. Furthermore, this result further indicates that the enhanced deformation kinetics in the FSP fine-grained aluminum alloys is associated with the high ratio of HAGBs, as shown in Fig. 2.

In order to enhance the understanding to the enhanced deformation kinetics, the variation of $\dot{\varepsilon}kT(d^{\text{eff}})^2/(G_gEb^3)$ versus σ/E for fine grained ECAP aluminum alloys from a literature [31] is shown in Fig. 14. The dimensionless constant was determined to be 40 and 300 for the alloys deformed at 400 °C and 500 °C, respectively. While the dimensionless constant of 40 is consistent with the prediction by Eq. (1), enhanced deformation kinetics was also observed in the ECAP aluminum alloys at higher temperatures. It was reported that with increasing annealing temperature, accompanied by the increase in the grain size, the fraction of HAGBs in ECAP aluminum alloys increased [32,33]. Clearly, the increase in the dimensionless constant for the ECAP aluminum alloys should be attributed to the increase in the fraction of HAGBs at 500 °C when the d^{eff} was used. This further support our suggestion that high value of dimensionless constant, i.e. enhanced kinetics of GBS, in the FSP aluminum alloys is caused by high percent of HAGBs, and the true dimensionless constant can be obtained by using the d^{eff}.

5. Conclusions

1. Three differently grained (1.6, 2.6 and 2.9 μm) Al–Mg–Sc samples with similar grain shape, misorientation distribution and texture were produced through changing FSP parameters, which

ensured that the initial microstructure for superplastic investigation differed only in the grain size.

2. A conception of effective grain size (d^{eff}), i.e. the grain size just before deformation, was proposed. At a given temperature, the superplasticity was governed by the d^{eff} rather than the initial grain size d^{ini}. Furthermore, a concentrative d^{eff} distribution was beneficial to increasing the superplastic elongation and optimum strain rate despite the same d^{eff}.
3. The aluminum alloys with a fine d^{ini} usually exhibited a smaller d^{eff} and excellent superplasticity at lower temperatures but a significantly reduced superplasticity at higher temperatures. The aluminum alloys with a medium d^{ini} exhibited the largest superplastic elongation and the highest strain rate due to its lowest d^{eff} at a moderate temperature. The aluminum alloys with a coarse d^{ini} could show a high superplastic elongation at a high temperature.
4. A modified constitutive equation with the d^{eff} was developed to predict the superplastic behavior at higher temperatures. The breakdown of the traditional constitutive equation is due to significant grain growth at higher temperatures.
5. The large variation range in the dimensionless constant for the FSP aluminum alloys is associated with the use of the d^{ini} in constitutive relationship for superplasticity. By using the d^{eff}, the true dimensionless constant was obtained, which further supports the suggestion that enhanced kinetics of GBS was associated with the high fraction of HAGBs.

Acknowledgement

The authors gratefully acknowledge the support of the National Natural Science Foundation of China under grant nos. 5087111, 50671103 and 50890171.

References

[1] T.G. Langdon, Metall. Trans. 13A (1982) 689–701.
[2] R.S. Mishra, T.R. Bieler, A.K. Mukherjee, Acta Metall. Mater. 43 (1995) 877–891.
[3] A. Arieli, A.K. Mukherjee, Mater. Sci. Eng. A 45 (1982) 61–70.
[4] Z. Horita, M. Furukawa, M. Nemoto, A.J. Barnes, T.G. Langdon, Acta Mater. 48 (2000) 3633–3640.
[5] F. Musin, R. Kaibyshev, Y. Motohashi, G. Itoh, Scripta Mater. 50 (2004) 511–516.
[6] S. Komura, Z. Horita, M. Furukawa, M. Nemoto, T.G. Langdon, Metall. Mater. Trans. 32A (2001) 707–716.
[7] Z. Horita, T.G. Langdon, Scripta Mater. 58 (2008) 1029–1032.
[8] R. Kaibyshev, E. Avtokratova, A. Apollonov, R. Davies, Scripta Mater. 54 (2006) 2119–2124.
[9] T.G. Nieh, L.M. Hsiung, J. Wadsworth, R. Kaibyshev, Acta Mater. 46 (1998) 2789–2800.
[10] R. Kaibyshev, F. Musin, D.R. Lesuer, T.G. Nieh, Mater. Sci. Eng. A 342 (2003) 169–173.
[11] Z.Y. Ma, R.S. Mishra, M.W. Mahoney, Acta Mater. 50 (2002) 4419–4430.
[12] V.N. Chuvil'deev, A.V. Shchavleva, A.V. Nokhrin, O.É. Pirozhnikova, M.Y. Gryaznov, Y.G. Lopatin, A.N. Sysove, N.V. Melekhin, N.V. Sakharo, V.I. Kopylov, M.M. Myshlyaev, Phys. Solid State 52 (2010) 1098–1106.
[13] Z.Y. Ma, R.S. Mishra, M.W. Mahoney, R. Grimes, Metall. Mater. Trans. 36A (2005) 1447–1458.
[14] F.C. Liu, Z.Y. Ma, Scripta Mater. 59 (2008) 882–885.
[15] I. Charit, R.S. Mishra, Acta Mater. 53 (2005) 4211–4223.
[16] Z.Y. Ma, R.S. Mishra, Scripta Mater. 53 (2005) 75–80.
[17] F.C. Liu, Z.Y. Ma, L.Q. Chen, Scripta Mater. 60 (2009) 968–971.
[18] F.C. Liu, Z.Y. Ma, Scripta Mater. 58 (2008) 667–670.
[19] F.C. Liu, Z.Y. Ma, Scripta Mater. 62 (2010) 125–128.
[20] Z.Y. Ma, F.C. Liu, R.S. Mishra, Acta Mater. 58 (2010) 4693–4704.
[21] R. Raj, A.K. Ghosh, Acta Metall. Mater. 29 (1981) 283–292.
[22] N. Chandra, J. Rama, P. Dang, Mater. Sci. Eng. A 231 (1997) 134–142.
[23] P. Dang, N. Chandra, Acta Mater. 46 (1998) 2851–2857.
[24] J.K. Mackenzie, Biometrika 45 (1958) 229–240.
[25] Kh.A.A. Hassan, A.F. Norman, D.A. Price, P.B. Prangnell, Acta Mater. 51 (2003) 1923–1936.
[26] A.P. Gerlich, T. Shibayanagi, Scripta Mater. 60 (2009) 236–239.
[27] R.Z. Valiev, A.V. Korznikov, R.R. Mulyukov, Mater. Sci. Eng. A 168 (1993) 141–148.
[28] J.W. Edington, K.N. Melton, C.P. Cutler, Prog. Mater. Sci. 21 (1976) 63–170.
[29] L.B. Johannes, R.S. Mishra, Mater. Sci. Eng. A 464 (2007) 255–260.
[30] F.C. Liu, Z.Y. Ma, J. Mater. Sci. 44 (2009) 2647–2655.
[31] S. Lee, A. Utsunomiya, H. Akamatsu, K. Neishi, M. Furukawa, Z. Horita, T.G. Langdon, Acta Mater. 50 (2002) 553–564.
[32] D.G. Morris, M.A. Muñoz-Morris, Acta Mater. 50 (2002) 4047–4060.
[33] M. Reihanian, R. Ebrahimi, M.M. Moshksar, D. Terada, N. Tsuji, Mater. Charact. 59 (2008) 1312–1323.